ELSEVIER

Contents lists available at ScienceDirect

Journal of Materials Science & Technology

journal homepage: www.elsevier.com/locate/jmst



Research Article

Truss-inspired ultra-high strength, fire-safe, and thermal insulating double-crosslinked wood aerogels



Yue Xu^{a,b,d}, Shuhui Liang^b, Wanying Wang^b, Chentao Yan^{b,d}, Lubin Liu^{b,d,*}, Dawei Jiang^{b,d}, Min Hong^c, Miaojun Xu^{a,b,d,*}, Bin Li^{a,b,d}, Siqi Huo^{c,*}

- ^a Key Laboratory of Bio-based Material Science and Technology, Ministry of Education, Northeast Forestry University, Harbin 150040, China
- ^b Heilongjiang Key Laboratory of Molecular Design and Preparation of Flame Retarded Materials, College of Chemistry, Chemical Engineering and Resource Utilization. Northeast Forestry University, Harbin 150040, China
- ^c School of Engineering, Centre for Future Materials, University of Southern Queensland, Springfield 4300, Australia
- d Key Laboratory of Forest Plant Ecology, Ministry of Education, Northeast Forestry University, Harbin 150040, China

ARTICLE INFO

Article history: Received 12 August 2025 Revised 25 September 2025 Accepted 25 September 2025 Available online 15 October 2025

Keywords: Bionic wood-based aerogel Fire safety Mechanical strength Thermal insulation Flame retardant mechanism

ABSTRACT

Bio-based wood aerogel is one of the most promising materials to replace traditional petrochemical-based insulation materials. However, the flammability and poor mechanical strength of bio-based wood aerogels limit their applications in emerging fields. Inspired by a truss-supporting system, this study prepared a multifunctional bio-based cross-linked wood aerogel (TSP@Ca) by a dual hydrogen-ionic bonding strategy involving an oxidized wood cellulose framework, sodium alginate, phytic acid (PA), and Ca2+. Finite element simulation and mechanical analysis indicated that the multi-point support structure, resembling a truss framework, formed in the oxidized wood template significantly improved the strength of TSP@Ca aerogel (9.99 MPa), with a 154.84 % enhancement relative to that of oxidized delignified wood (TODW). The limiting oxygen index of TSP@Ca3 aerogel was as high as 43.3 %, and it can extinguish immediately when the fire was removed. The introduction of PA and Ca²⁺ promoted the dehydration, cross-linking, and charring of TSP@Ca aerogel, while the produced phosphorus-containing free radicals played an inhibitory role in the gas phase. Therefore, the peak of heat release rate of TSP@Ca aerogel was 80.66 % lower than that of TODW, showing excellent fire safety. Benefiting from the complex heat conduction path and enhanced interface resistance, the thermal conductivity of TSP@Ca was 46.4 % lower than that of TODW. The resulting aerogel combines ultra-high mechanical strength, excellent fire resistance, and thermal insulation, aligning with "green" development goals and offering broad application potential in construction, rail transport, and new energy sectors.

© 2025 Published by Elsevier Ltd on behalf of The editorial office of Journal of Materials Science & Technology. This is an open access article under the CC BY license (http://creativecommons.org/licenses/by/4.0/)

1. Introduction

With the rapid development of the global economy, the energy crisis driven by excessive energy consumption is becoming increasingly severe. It is reported that about 40 % of the world's total energy usage is attributed to building insulation needs [1–3]. Currently, the most effective method to improve building insulation is the application of petrochemical-based insulation materials, including rigid polyurethane foam (RPUF) and expandable polystyrene foam (EPS), on the walls [4,5]. However, these insulation materials are highly flammable, and they present significant

E-mail addresses: liulubin@nefu.edu.cn (L. Liu), xumiaojun@nefu.edu.cn (M. Xu), sqhuo@hotmail.com, Siqi.Huo@unisq.edu.au (S. Huo).

drawbacks, such as environmental pollution, poor degradability, and unsustainable production processes, which have caused irreversible adverse impacts on global sustainable development [6,7]. Therefore, bio-based thermal insulation materials derived from natural, renewable resources have attracted growing attention as promising alternatives.

As a natural hollow tubular bio-based material, wood has been widely used in emerging construction, rail transportation, and home decoration [8–10]. Among various species, balsa wood stands out as an ultra-light material with excellent thermal and sound insulation [11,12]. After delignification, balsa wood can be transformed into oriented and functional cellulose aerogels [13]. For instance, He et al. selectively oxidized the hydroxyl groups of cellulose C6 to carboxyl groups by the 2,2,6,6-tetramethylpiperidinooxy (TEMPO)-mediated system and then deposited polypyrrole onto

^{*} Corresponding authors.

the surface to prepare conductive aerogels for supercapacitors [14]. However, cellulose aerogels generally exhibit inferior mechanical properties compared to pure wood. Current strategies to enhance functionality often involve anionizing cellulose to modulate electrostatic repulsion between microfibers, promoting further modification [15–17]. Nevertheless, delignified wood (DW) aerogels still suffer from low mechanical strength, and it is difficult to achieve satisfactory mechanical strength by simple structural reconstruction. Meanwhile, they are highly flammable and accompanied by smoldering due to their cellulose-rich composition, necessitating flame-retardant treatments for most applications [18].

Flame retardancy of cellulose aerogels can be improved by adding inorganic, phosphorus-based, phosphorus-nitrogen, and intumescent flame retardants [19-22]. Wu et al. [23] introduced sepiolite (SEP) into the cellulose aerogel, significantly enhancing the thermal stability and flame retardancy of cellulose nanofibers/SEP. Unfortunately, the high density of these flame retardants often compromises the lightweight and thermal insulation of cellulose aerogels [24]. Besides, the poor compatibility between flame retardants and cellulose aerogels can further reduce mechanical properties [25]. Recent studies have shown that a dual cross-linked structure can enhance the mechanical strength of flame-retardant cellulose aerogels [26-28]. For example, Zhu et al. developed a cellulose nanofiber/alginate/boric acid composite aerogel using a directional freezing method [29]. Alginate and boric acid were used as dual crosslinkers and flame retardants, increasing the axial stress from 72.6 to 300.8 kPa. However, this value remains far below the strength required for practical use.

It is well known that spider webs in nature have a stable structure composed of radial and circular fibers that can effectively distribute loads [30]. In addition, the lightweight hollow structure of bird bones and the vein distribution of leaves all reflect the strategy of optimizing the mechanical distribution of materials by the combination of rods [31-34]. The truss structure derived from the above natural phenomena is widely used in high-rise buildings for their uniform load distribution and high bearing capacity [35-38]. Therefore, we envisioned that introducing a staggered, truss-like support network within the hollow channels of wood could significantly reinforce cellulose aerogels. Herein, inspired by the truss structure, we developed a multifunctional bio-based cross-linked wood aerogel by a dual cross-linking (hydrogen and ionic bonding) strategy. Using sol-gel and ion-exchange processes, sodium alginate, phytic acid (PA), and Ca²⁺ were integrated into the oxidized wood template to form a multi-point support structure analogous to a truss framework. This structure not only imparted high mechanical strength to TSP@Ca aerogel but also effectively limited the internal heat transfer during combustion. Therefore, the prepared wood-based bionic aerogel combines excellent fire safety, mechanical strength, light weight, and thermal insulation, offering a novel pathway toward advanced, multifunctional wood-based aerogels for high-end applications.

2. Experimental section

2.1. Materials

Balsa wood is produced in Papua New Guinea. Sodium alginate (SA) and sodium chlorite (NaClO₂, purity \approx 80 %) were purchased from McLean Biochemical Technology Co., Ltd. (Shanghai, China). Calcium chloride powder (CaCl₂, 94 %) was provided by Energy Chemical Co., Ltd. (Anhui, China). PA, glacial acetic acid (CH₃COOH), and TEMPO (98 %) were provided by Aladdin Biochemical Technology Co., Ltd. (Shanghai, China). Sodium bromide (NaBr, 99 %) was obtained from Roan Reagent Co., Ltd. (Shanghai, China). Hydrogen peroxide solution was purchased from Damao Chemical Reagent Co., Ltd. (Tianjin, China). Sodium hypochlorite

(NaClO, effective chlorine content ≥ 10.0 %) was purchased from Tianli Chemical Reagent Co., Ltd. (Tianjin, China).

2.2. Preparation of DW and TEMPO-oxidized wood aerogels

First, the control wood samples were cut into the required size and delignified by soaking in 2 wt. % NaClO_2 and acetic acid solution (pH =4.6) at 80 °C for 5 h. After that, the samples were immersed in 20 wt. % H_2O_2 solution at 80 °C for 30 min to further remove the residual lignin and part of the hemicellulose. The samples were rinsed with deionized water 3–5 times and freeze-dried to obtain DW.

Then, selectively oxidized the DW was TEMPO/NaBr/NaClO system with a mass ratio of 100:1 for DW and TEMPO [14,15]. The oxidation times of TEMPO were set at 1, 2, 3, 4, 5, and 6 h, respectively (Fig. S1-S3 in the Supplementary Materials). After the completion of each oxidation, the reaction was terminated by adding anhydrous ethanol and washed with deionized water to a pH = 7. The oxidized DW was denoted as TODW, and the samples with different reaction times were freezedried and named as TODW1, TODW2, TODW3, TODW4, TODW5, and TODW6, respectively. The optimal TEMPO oxidation times were selected based on the surface morphology and mechanical properties of the samples (Supplementary Materials).

2.3. Preparation of wood-based aerogels

First, sodium alginate (SA) solutions with concentrations of 0.4, 0.8, 1.2, 1.6, and 2.0 wt. % were prepared (Fig. S4 and Supplementary Materials). The SA solution was vacuum pressure-impregnated into the TODW obtained above for 3 h. The samples were then frozen at $-18~^{\circ}\text{C}$ for 12 h and ion-exchanged in a 3 % CaCl $_2$ ethanol solution at 18 $^{\circ}\text{C}$ for 24 h. After that, the samples were removed and placed in deionized water for a long time with several water changes to wash off the unreacted CaCl $_2$ on their surface and inside. Finally, the samples were freeze-dried to obtain TS@Ca.

Second, 1.2 % SA solution was prepared, and PA was added according to the SA:PA (functional group ratio) of 1:1, 1:2, 1:3, and 1:4, respectively. After stirring evenly, the SA/PA mixture was vacuum pressure-impregnated into TODW. Then the above steps were repeated for Ca²⁺ replacement. After freeze-drying, the final aerogel samples were obtained and named as TSP@Ca1, TSP@Ca2, TSP@Ca3, and TSP@Ca4. The detailed preparation method is shown in Fig. 1.

2.4. Characterization

The structural morphology and elemental composition of the TSP@Ca aerogel were characterized by scanning electron microscope (SEM), Fourier transform infrared spectroscopy (FTIR), and X-ray photoelectron spectroscopy (XPS). The mechanical properties of flame-retardant TSP@Ca aerogel composites were studied, and their reinforcement mechanism was analyzed by finite element simulation. The thermal conductivity test and thermal infrared imaging test were utilized to explore the thermal insulation performance of aerogel. The flame retardancy and combustion performance of aerogel were carried out by vertical burning (UL-94), limiting oxygen index (LOI), and cone calorimetry (CC) tests. In addition, the char residues after combustion of the samples were analyzed by FTIR, SEM, XPS, and thermogravimetric analysisinfrared spectrometry (TG-IR), and the flame retardant mechanism of TSP@Ca was revealed. The details are provided in the Supplementary Materials.

The density of TSP@Ca aerogel was calculated by Eq. (1), where m is the mass, and V is the volume of the corresponding sample. The porosity was calculated by the mass method according to

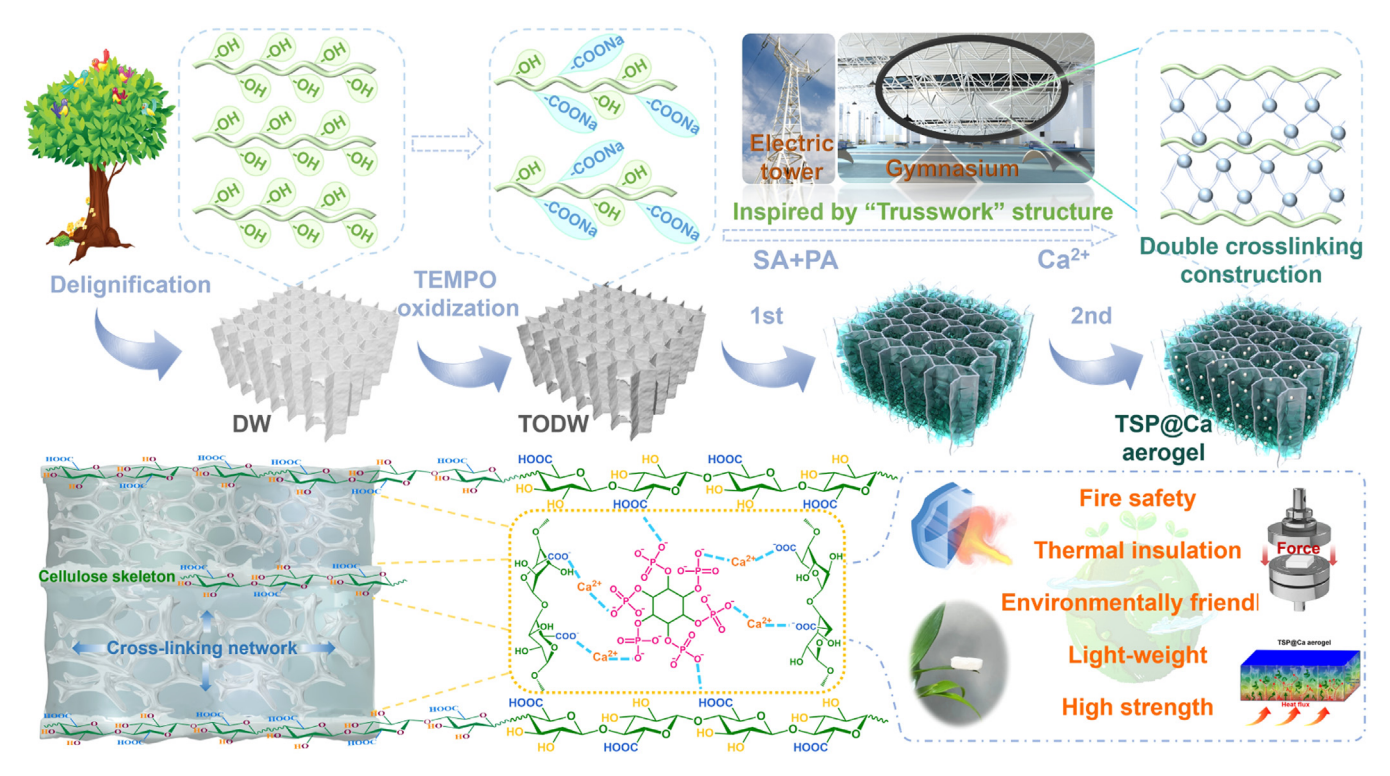


Fig. 1. Schematic diagram of the preparation of TSP@Ca aerogel.

Eq. (2). First, the aerogel sample was weighed (m_1) and placed in a container filled with ethanol with a total weight of m_2 . Then, the container was placed in a vacuum oven with the vacuum treatment until no bubbles emerge from the sample. After removing the sample from the container, the weight of the container with the remaining ethanol was recoeded as m_3 .

$$\rho = \frac{m}{V} \tag{1}$$

Porosity (%) =
$$\frac{m2 - m3 - m1}{m2 - m3} \times 100$$
 (2)

3. Results and discussion

3.1. Preparation and structural analysis of wood-based aerogel

In this work, mimicking the truss structure supporting system, the C6 of delignified natural balsa wood was selectively oxidized by the TEMPO/NaBr/NaClO system, and the mixture of SA and PA was vacuum pressure-impregnated into TODW by imitating the truss structure supporting system. After cryo-Ca²⁺ replacement and freeze-drying, a bio-based double cross-linked wood aerogel was obtained (Fig. 1). Compared with the hydrogen bonding between traditional polysaccharide materials [39,40], the introduction of Ca²⁺ enables TODW, SA, and PA to form a supporting structure of ion-crosslinked aerogel in the wood template. It not only maintains the low thermal conductivity of TSP@Ca wood aerogel, but also effectively improves its mechanical and lightweight properties. Meanwhile, the cross-linking and flame-retardant reinforcing agents Ca²⁺ and PA endow TSP@Ca wood aerogel with excellent fire safety performance. Compared with the original SA aerogel, TSP@Ca aerogel shows good water resistance (Fig. S5). This is equivalent to constructing a truss-like structure support with double cross-linking of Ca2+ and hydrogen bonds in the wood frame, expanding the application of traditional bio-based timber

in emerging areas such as construction materials, new energy, and rail transportation.

The morphologies of original wood, DW, TODW, and TSP@Ca aerogels were observed by SEM. According to Fig. 2(a), the natural tubes of the original wood are evenly distributed with a pentagonal or hexagonal structure and uniform tube wall thickness. After lignin removal and TEMPO oxidation treatment, it can be seen clearly that the tube wall of TODW further becomes thinner and wrinkled, and some cracks and lines appear on the tube wall (Fig. 2(b)). This creates favorable conditions for the subsequent construction of 3D network structures within the tube. After the introduction of SA, PA, and Ca²⁺, a truss-like supporting system is obviously formed inside the natural hollow tubes of the wood (Figs. 2(c) and S6). Meanwhile, the uniform distribution of phosphorus and Ca²⁺ can be seen by energy dispersive X-ray (EDS)-Mapping (Fig. 2(d)). The FTIR results of TSP@Ca aerogel are shown in Fig. 2(e). From the FTIR spectrum of wood, the broad peak at $3348~cm^{-1}$ belongs to the -OH group. The characteristic peaks of lignin at 1456, 1503, and 1593 cm^{-1} disappear after the natural balsa wood was treated with sodium chlorite solution, indicating the successful removal of lignin. The peaks at 1732 and 1237 cm⁻¹ are significantly weakened, which is attributed to the partial removal of hemicellulose. After TEMPO oxidation system treatment, the enhancement of characteristic peaks of the carboxylic acid group (1732 and 1596 cm⁻¹) indicates that the -OH at the C6 position of cellulose has been oxidized to -COOH. With the introduction of SA, PA, and Ca²⁺, the FTIR spectrum of TSP@Ca3 has a new asymmetric stretching vibration peak of P-O-C at 1003 cm⁻¹. In addition, the broad peak of -OH (3322 cm⁻¹) of TSP@Ca3 obviously shifts to the low band, and its carboxyl vibration peak at 1596 cm⁻¹ is further enhanced, indicating the formation of Ca²⁺ and hydrogen bond double cross-linking structure in TSP@Ca3.

To further analyze the microstructure and chemical composition of the TSP@Ca aerogels, the XPS tests of DW, TODW, and TSP@Ca3 aerogels were performed (Figs. 2(f-i) and S7). After oxidation in the TEMPO/NaBr/NaClO system, the proportion of C-O and C=O in

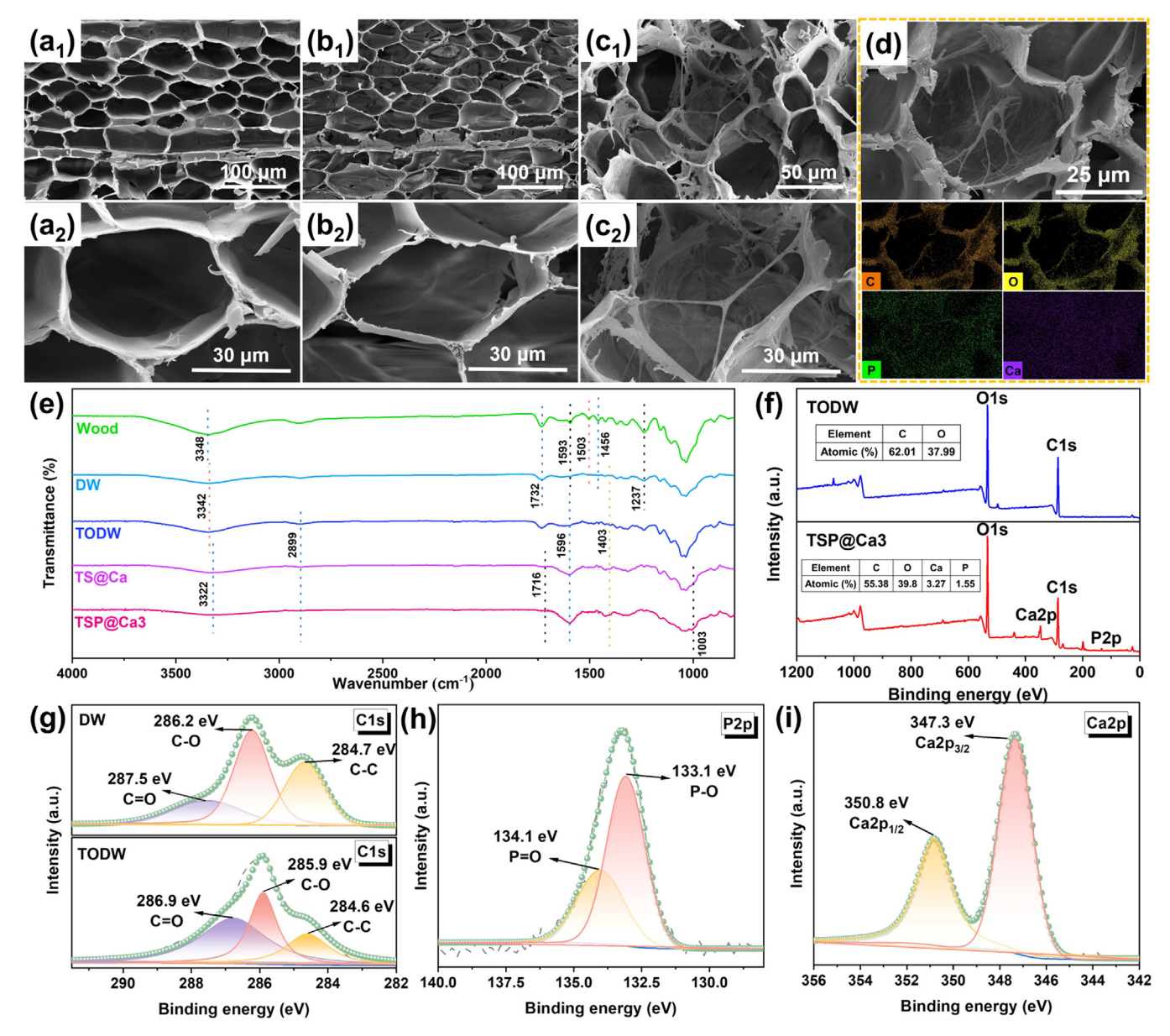


Fig. 2. Structural characterization of the samples. (a) SEM images of wood. (b) SEM images of TODW. (c) SEM images of TSP@Ca3. (d) EDS Mapping images of TSP@Ca3. (e) Infrared spectra of wood, DW, TODW, TS@Ca, and TSP@Ca3. (f) XPS spectrum of TODW and TSP@Ca3. (g) XPS high-resolution C 1s spectrum of DW and TODW. (h) XPS high-resolution P 2p spectrum of TSP@Ca3 aerogel. (i) XPS high-resolution C a 2p spectrum of TSP@Ca3 aerogel.

TODW is significantly higher than that in DW, and the peaks of C–O and C=O move toward lower binding energy due to the newly formed hydrogen bonds. With the introduction of the double cross-linked structure, TSP@Ca3 obviously adds Ca and P element peaks, and its O content increases from 38.0 % of TODW to 39.8 % due to the presence of oxygen-rich SA and PA. In the P 2p spectrum of TSP@Ca3, the peaks at 134.1 and 133.1 eV belong to P=O and P-O, respectively. Meanwhile, the Ca 2p peaks at 347.3 and 350.8 eV correspond to Ca $2p_{3/2}$ and Ca $2p_{1/2}$, respectively, demonstrating that the Ca valence of the TSP@Ca aerogel structure is +2. The above analysis further proves the successful preparation of TSP@Ca truss-structured aerogel.

3.2. Mechanical performance and simulation mechanism analysis

Generally, the strength of traditional wood tends to decrease significantly after being processed (Fig. 3(a and b)). After delignification and oxidation of NW, the compressive strength of TODW

is decreased by 36.77 % compared with NW. With the introduction of the double cross-linked network, the mechanical properties of TSP@Ca aerogel materials are significantly improved. The compressive strength of TSP@Ca1, TSP@Ca2, and TSP@Ca3 is 9.47, 9.53, and 9.99 MPa, which is 141.58 %, 143.11 %, and 154.84 % higher than those of TODW, respectively. When the ratio of SA:PA increases to 1:4, the molecular interaction force between the SA/PA mixture intensifies, and their viscosity becomes too high, resulting in difficult impregnation of TSP@Ca4 (Fig. S8). Thus, TSP@Ca3 aerogel also maintains excellent lightness due to the construction of its internal truss-like structure reinforcement system. It can not only stand on the leaf surface of the plant to remain stable but also can withstand two people (178 kg) standing on it without deformation (Fig. 3(c and d)).

To further prove the structural reinforcement mechanism of TSP@Ca aerogel, the stress-strain during the compression process was explored by finite element simulation (Figs. 3(e) and S9 and Supplementary Materials). When the naturally hollow pipe

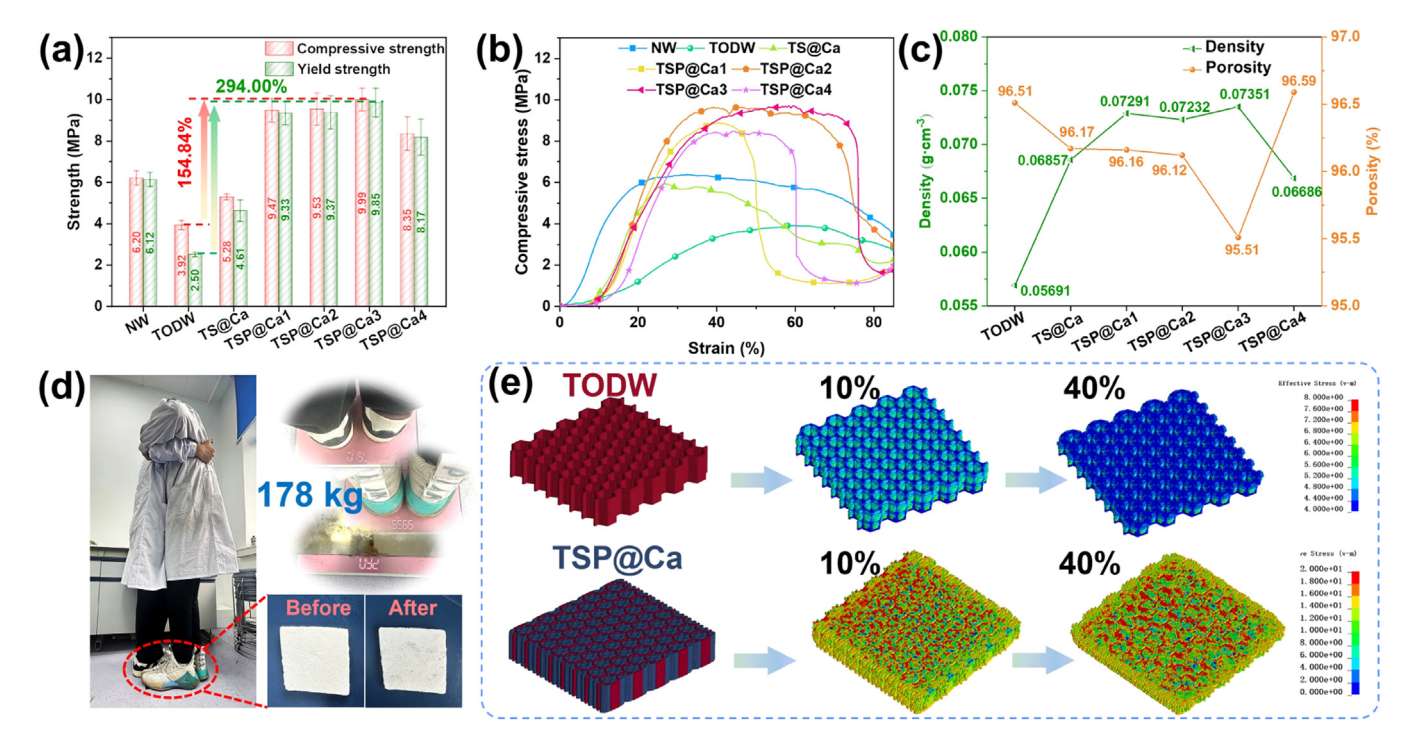


Fig. 3. (a) Maximum compressive strength and yield strength of NW, TODW, TS@Ca, and TSP@Ca aerogels. (b) Stress-strain curves of NW, TODW, TS@Ca, and TSP@Ca aerogels. (c) Density and porosity curves of NW, TODW, TS@Ca, and TSP@Ca aerogels. (d) Load-bearing display photos of TSP@Ca3 aerogel with a dimension of 5 cm × 5 cm × 0.4 cm. (e) Finite element simulation of compression process of TODW and TSP@Ca aerogels.

of TODW is subjected to downward pressure, the radial tubular structure wrinkles and even deforms. However, after constructing a truss-like structure in the natural pipe, the radial tubular structure not only provides better support for the pressure, but the truss-like structure inside the pipe also disperses the pressure, thereby giving TSP@Ca aerogel excellent compressive strength. Meanwhile, the internal energy of the finite element simulation is compared (Fig. S9). The greater increase in internal energy proves that the same compression requires more energy input, which indicates a higher compressive strength. This indicates that compared with NW, the bionic truss-structured TSP@Ca aerogel requires higher internal energy to destroy its structure, therefore, it has higher mechanical properties.

3.3. Fire safety analysis

Generally, natural polymer materials are highly flammable, which limits their application in electronics, electrical appliances, rail transit, and other fields. Therefore, the flame retardant properties of TODW, TS@Ca, and TSP@Ca aerogel materials were studied by UL-94 and LOI tests (Fig. 4 and Table S1). Once TODW is ignited, it burns rapidly without burning level and its LOI value of only 27.7 %. With the introduction of SA and Ca²⁺, the burning time of TS@Ca aerogel is significantly prolonged, and its LOI increases to 38.2 %. Due to the introduction of phosphorus-rich PA and the formation of a double cross-linked network, TSP@Ca2 and TSP@Ca3 aerogels not only obtain the UL-94 V-0 rating, but also the LOI of TSP@Ca aerogel is obviously improved with the increase of PA ratio. The LOI values of TSP@Ca2 and TSP@Ca3 are 41.9 % and 43.3 %, which are 51.3 % and 56.3 % higher than those of traditional wood.

To further explore the effect of the introduction of SA, Ca^{2+} , and PA on the combustion behavior of TODW aerogel, the CC tests were carried out on TODW, TS@Ca, and TSP@Ca aerogels (Figs. 4(b)–(d) and S10–S13, and Table S2). After DW is oxidized, TODW is easy to burn, and its Time to ignition (TTI) is only 4 s. With the introduction of Ca^{2+} and PA, the TTI of TSP@Ca aerogel is substantially

improved. The TTI of TSP@Ca3 reaches 18 s, which indicates that it has a higher ignition threshold. TODW quickly reaches peak of heat release rate (PHRR) (946.8 kW/m²) at 24 s, and its THR (total heat release) is 38.5 MJ/m². The introduction of SA and Ca²+ reduces the THR of TS@Ca to 29.9 MJ/m², but still maintains a high PHRR (507.3 kW/m²). Interestingly, the HRR of TSP@Ca aerogels significantly decreases with the introduction of PA. The PHRR of TSP@Ca3 is reduced by 80.66 % compared with TODW. This is attributed to the fact that the introduction of PA not only enables TS@Ca to form a double cross-linked network structure but also promotes the cross-linking carbonization of the TSP@Ca matrix during combustion. Therefore, the THR of TSP@Ca3 is reduced to 13.2 MJ/m². Meanwhile, the catalytic charring of PA and the shielding effect of the char layer make the smoke produce rate (SPR) of TSP@Ca obviously lower than that of TODW.

In addition, after CC tests, the FPI, FGI, and FRI were calculated based on the test results and the following Eqs. (3-5). FPI and FGI represent the fire risk and flame spread rate of the material during combustion, respectively, while FRI is an important parameter for quantifying the flame retardant properties of composites [41–43]. As shown in Fig. 4(f) and Table S2, the FPI and FGI of TODW are $0.004~\text{m}^2~\text{s/kW}$ and $39.5~\text{kW}~\text{m}^{-2}/\text{s}$. With the introduction of PA and Ca²⁺, the FPI of TSP@Ca is obviously increased, while its FGI is decreased. The FPI of TSP@Ca3 (0.098 s m²/kW) is 24.5 times that of TODW, while its FGI is reduced to 1/8 of that of TODW. Moreover, the FRI (68.1) of TSP@Ca3 is 68 times higher than TODW. Compared with traditional TODW, the fire risk of TSP@Ca is obviously reduced. These findings collectively indicate that TSP@Ca not only improves the flame retardancy of composites but also greatly reduces the overall fire risk, which is a major breakthrough in making better and safer bio-based aerogels.

$$FPI = \frac{TTI}{PHRR}$$
 (3)

$$FGI = \frac{PHRR}{t_{\text{DUDP}}} \tag{4}$$

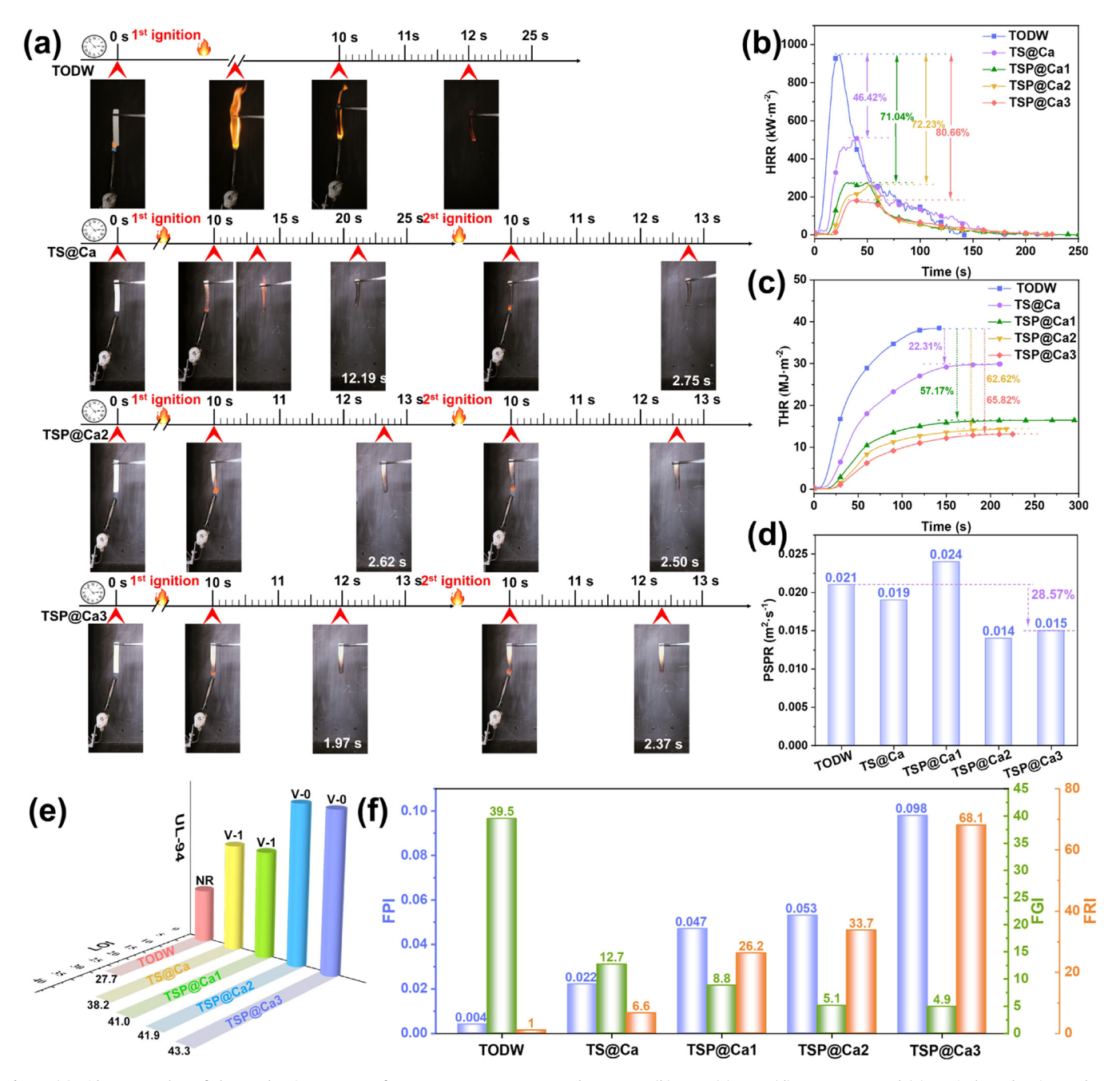


Fig. 4. (a) Video screenshot of the combustion process of TODW, TS@Ca, TSP@Ca2, and TSP@Ca3. (b) HRR, (c) THR, (d) SPR curves, and (e) vertical combustion and LOI distribution diagram of TODW, TS@Ca, TSP@Ca1, TSP@Ca2, and TSP@Ca3 aerogels. (f) Fire performance index (FPI), fire growth index (FGI), and flame retardancy index (FRI) after CC tests.

$$FRI = \frac{\left[THR \times \left(\frac{PHRR}{TTI}\right)\right]_{Neat\ TODW}}{\left[THR \times \left(\frac{PHRR}{TTI}\right)\right]_{Aerogel\ composites}}$$
 (5)

3.4. Flame retardant mechanism analysis

After CC testing, the microstructure and chemical composition of the residual char are important bases for analyzing the condensed-phase flame retardancy of the material. After strong thermal radiation, pure TODW only left a trace amount of white residue, and its original wood frame structure collapsed obviously (Fig. 5(a)). Compared with TODW, TS@Ca aerogel formed a continuous char layer after CC tests owing to the introduction of SA

and Ca²⁺, and the char layer obviously retained the fiber structure of the original wood frame. In comparison, the introduction of PA enables TSP@Ca to form a double-cross-linked structure with a truss-like skeleton. After CC testing, the volume and integrity of the residual char in TSP@Ca aerogel material were significantly improved (Fig. 5(a)). In addition, with the increase of PA introduction amount, the charring degree of wood framework fibers is significantly enhanced, which effectively plays a skeleton supporting role in the condensed phase (Figs. 5(b–e) and S14).

The chemical structure of the residual char of TODW, TS@Ca, and TSP@Ca aerogels was further analyzed by FTIR and XPS (Figs. 5(f-i) and S15). The char residue after TODW combustion is carbonate (υ CO₃²⁻: 1428 cm⁻¹, δ CO₃²⁻: 876 cm⁻¹). With the introduction of Ca²⁺ and PA, new –OH (3359 cm⁻¹) and C=C (1393

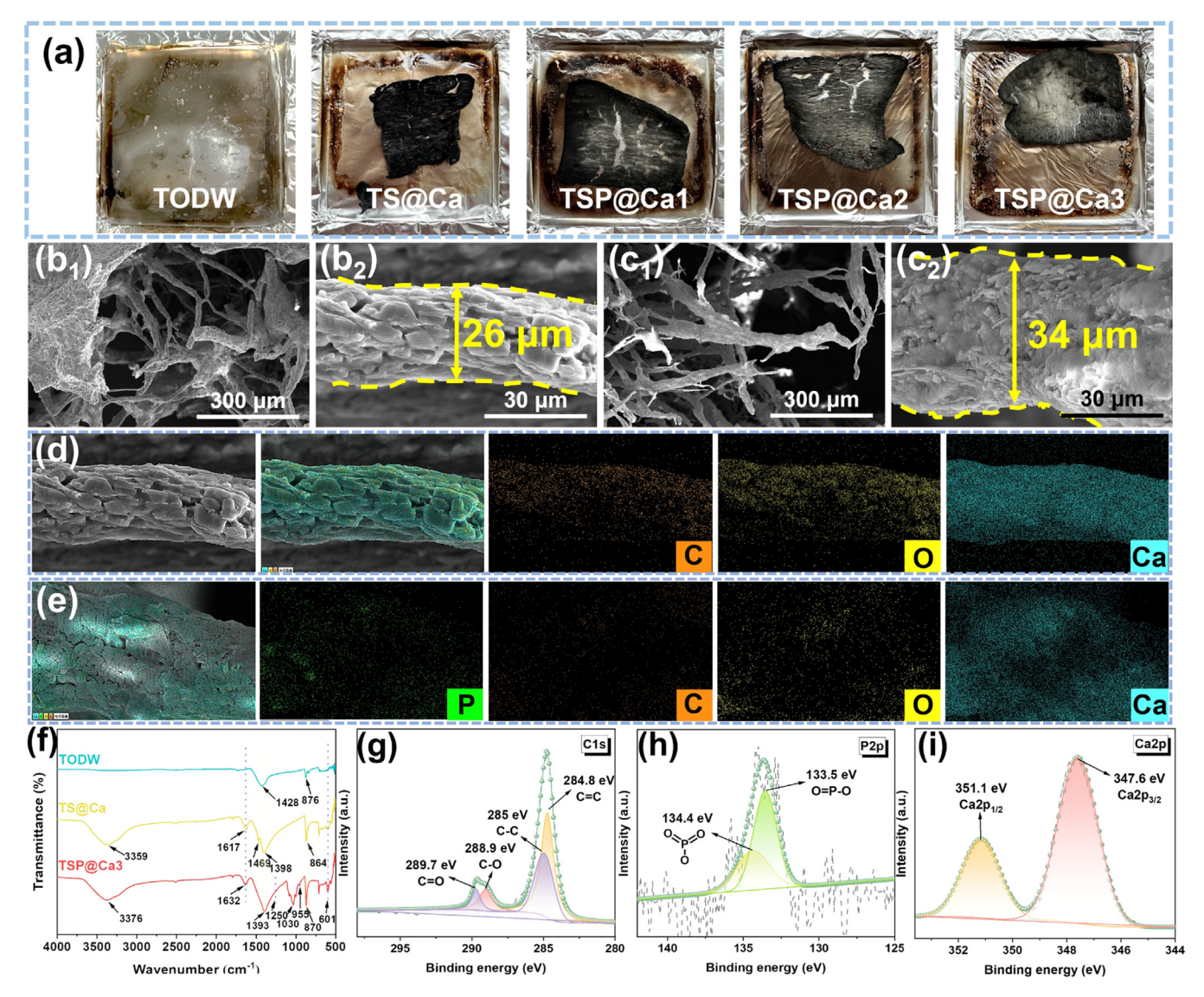


Fig. 5. (a) Digital photographs of TODW, TS@Ca, TSP@Ca1, TSP@Ca2, and TSP@Ca3 aerogels. SEM images of residual char after CC tests for (b) TS@Ca and (c) TSP@Ca3 aerogels. EDS Mapping of char residues for (d) TS@Ca and (e) TSP@Ca3 aerogels. (f) FTIR spectrum of condensed phase char layer of TODW, TS@Ca, and TSP@Ca3 aerogels. XPS spectrum of the char layer: (g) C 1s, (h) P 2p, and (i) Ca 2p spectrum of TSP@Ca3.

cm $^{-1}$) peaks are observed in the TS@Ca and TSP@Ca char residues. Meanwhile, the new peaks of TSP@Ca residual char at 1250 and 1030 cm $^{-1}$ are attributed to the stretching vibration peaks of P=O and P-O. This indicates that the introduction of Ca $^{2+}$ and PA promotes the cross-linking charring of TSP@Ca, and the formed residual char effectively plays a protective role in the condensed phase. In addition, EDS-mapping and XPS analysis show that P and Ca are uniformly dispersed in the char residue after the CC test. By splitting the P 2p peak, the peaks at 134.4 and 133.5 eV were attributed to PO $_3$ and O=P-O. The Ca 2p peaks at 351.1 and 347.6 eV prove the cross-linking effect of Ca $^{2+}$ in the char layer. Combined with the high-resolution spectrum of C 1s (Fig. 5(g)), the introduction of PA and Ca $^{2+}$ markedly improves the crosslinking degree and strength of wood fibers, playing an excellent shielding role in the condensed phase.

The gas phase products during the pyrolysis of TODW, TS@Ca, and TSP@Ca aerogels were analyzed by TG-IR (Figs. 6(a-g) and S16). The main pyrolysis products of pure TODW aerogel are water (3574 and 3730 cm $^{-1}$), carbon dioxide (2322 and 2360 cm $^{-1}$), CO (2186 cm $^{-1}$), carbonyl compounds (1794 and 1772 cm $^{-1}$), aliphatic compounds (988 and 1170 cm $^{-1}$)and aromatic compounds (1560,

and 1468 cm⁻¹) [44]. With the introduction of cross-linking agents Ca²⁺ and PA, the amount of total thermal pyrolysis products of TS@Ca and TSP@Ca aerogels decreases significantly. Compared with TODW, the release of C-H, C=O, aromatic, and C-O flammable small molecules in TSP@Ca aerogel is reduced. Meanwhile, new peaks of P=O and P-O are obviously detected at 1280 and 988 cm⁻¹. This indicates that the phosphorus-containing free radicals from the decomposition of TSP@Ca aerogel during the thermal degradation process effectively play the gas-phase free radical capture role. Besides, the construction of the double-cross-linked structure of TSP@Ca aerogel promoted the charring of the material matrix, and the large number of char layers played a shielding role in the condensed phase, thereby inhibiting the combustion reaction of the cellulose framework.

Based on the above analysis, the potential flame retardant mechanism of TSP@Ca aerogel during combustion is revealed in Fig. 6(h). Under strong radiation conditions, pure TODW is highly flammable and poses a major safety hazard in most application areas. With the construction of the double cross-linked network, the P· and PO· free radicals produced by the thermal decomposition of the phosphorus-containing groups in the TSP@Ca aerogel effec-

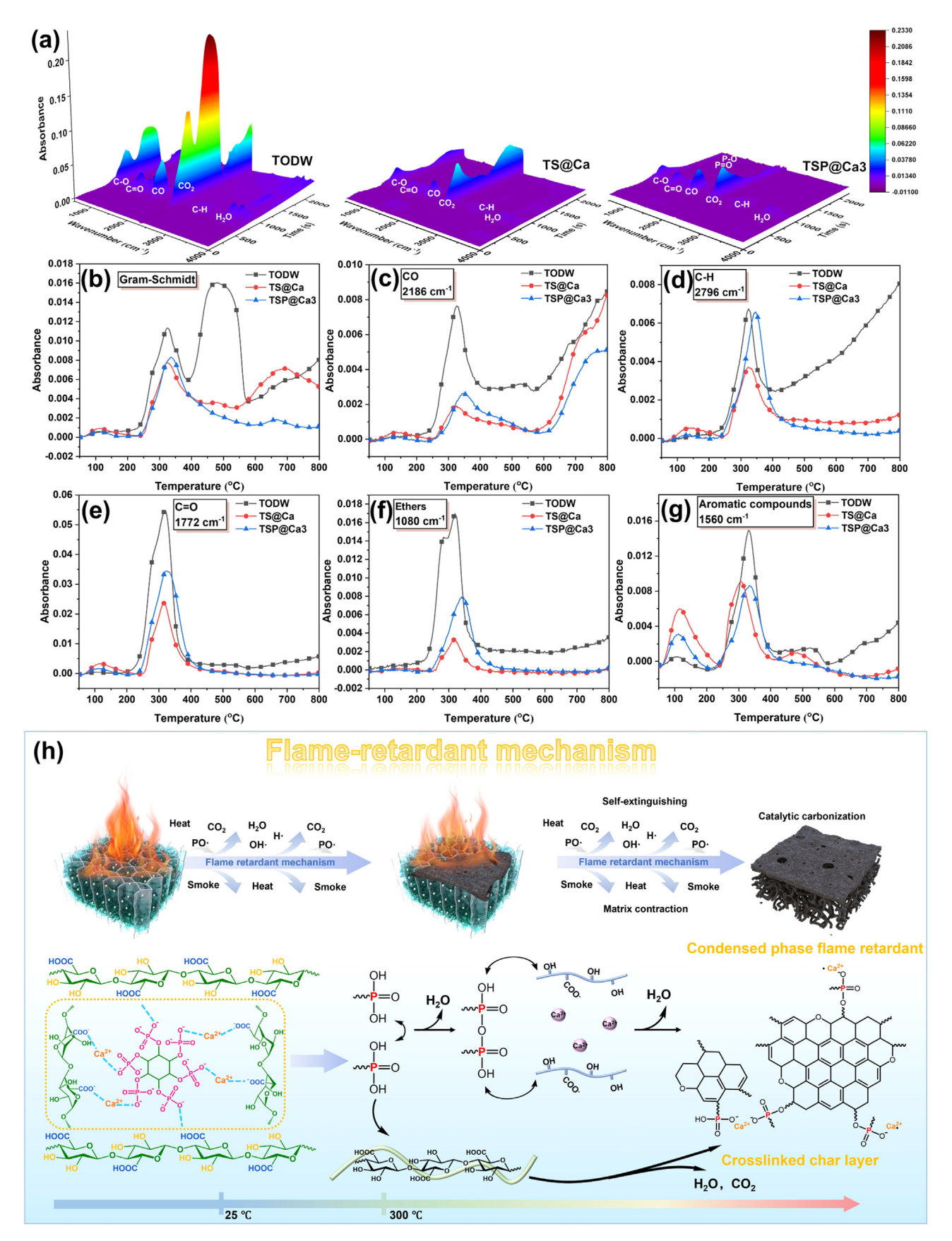


Fig. 6. Analysis of gas phase pyrolysis products of aerogels: (a) 3D TG-FTIR spectra of pyrolysis products for the TODW, TS@Ca, and TSP@Ca3. (b) Gram-Schmidt FTIR spectra of volatile products of TODW, TS@Ca, and TSP@Ca3. The absorption curves vs. temperature of (c) CO, (d) C-H, (e) C=O, (f) ethers, and (g) aromatic compounds for TODW, TS@Ca, and TSP@Ca3. (h) Speculated flame-retardant mechanism of TSP@Ca aerogels.

tively capture the $H\cdot$, $O\cdot$, and $OH\cdot$ released by the decomposition of TODW, thus interrupting the chain reaction required for sustained combustion. Furthermore, the metaphosphoric acid and pyrophosphoric acid produced by the decomposition of PA promote the dehydration and charring of the matrix. The formed char layer has high strength and density under the cross-linking of Ca^{2+} and phosphorus-containing compounds, which prevents the transfer of heat, oxygen, and combustible volatiles. In summary, TSP@Ca aerogel achieves excellent fire safety performance by the synergistic flame retardant effect of the gas phase and condensed phase.

3.5. Thermal insulation and application analysis

Traditional functional wood is mainly used in emerging construction, rail transit, and other fields. In addition to mechanical, flame-retardant, and other properties, thermal insulation performance is the key parameter for evaluating its application value. The axial and radial thermal conductivities of pure TODW are 0.1068 and 0.0495 W/(m K), and its average thermal conductivity is 0.0781 W/(m K) (Fig. 7(a)). With the introduction of the double network cross-linking structure, the thermal conductivity of TSP@Ca shows a transition from anisotropy to isotropy, gradually decreasing in the axial direction and remaining unchanged in the radial direction. Compared with TODW, the average thermal conductivity values of TSP@Ca1, TSP@Ca2, and TSP@Ca3 are 0.0663, 0.0642, and 0.0561 W/(m K), which are reduced by 15.1 %, 17.8 % and 28.2 %. The inferred thermal insulation mechanism enhanced by TSP@Ca aerogel is shown in Fig. 7(b). Generally, thermal conduction is controlled by thermal conduction, thermal convection (λ_c) , and thermal radiation (λ_r) [45]. For porous samples, λ_c can usually be neglected. Thermal conduction is classified into solid phase thermal conduction (λ_s) and gas phase thermal conduction (λ_g) . In pure TODW, the macropore structure of 30–60 μ m permits air molecules to circulate freely in the pores upon heating, thus achieving unrestricted thermal conduction. Therefore, for the original sample, heat is relatively easy to transfer due to the large pores and dense cell walls. Inversely, building double-crosslinked aerogels inside natural hollow tubes results in a complex structure that blocks most of the tubes and restricts the free motion of air molecules in the gas phase. Furthermore, the "island" structure of the composite aerogel not only makes the path of solid-phase heat transfer more complicated but also enhances the interface between the solid and the air, improving the reflectivity of heat radiation, thereby significantly decreasing λ_g , λ_s , and λ_r [46,47].

To further assess the thermal insulation performance of the aerogels under extreme conditions. TODW and TSP@Ca aerogel samples were exposed to a high temperature of 150 °C for analysis (Fig. 7(c)). The thermal image of the aerogel from top view and the curve of the top surface temperature of the sample changing with time are exhibited in Fig. 7(d and e). The surface temperature of the hot plate was maintained at 150 °C throughout the experiment. For TODW, when heated to 20 s, the upper surface temperature of the sample quickly rises to 95.6 °C, and by 100 s, the upper surface temperature of the sample gradually increases to 107.4 °C and remains stable. However, for TSP@Ca3, the upper surface temperature only increases to 80.5 °C at the beginning of 20 s, which decreases by 15.79 % compared with TODW. Keep heating to 100 s, the upper surface temperature of TSP@Ca3 aerogel increased slightly to only 89.2 °C, which is 16.95 % lower than that of TODW. Although the sample thickness is only 4 mm, TSP@Ca still exhibits excellent thermal insulation performance in a hightemperature environment. Meanwhile, to more intuitively explore the thermal insulation performance of aerogels in practical applications, a thermal insulation house model was built (Fig. 7(f and g)). The ambient temperature was 18 °C, and 100 °C hot water was placed in different sample models (air, TODW, and TSP@Ca3). It can be seen obviously from the temperature curves that the overall cooling trend is fast at first and then slow. However, the temperature of TSP@Ca3 drops the slowest. Especially in 1000–8000 s, the gap between the TSP@Ca3 with air and TODW is the largest. Therefore, TSP@Ca3 aerogel has excellent thermal insulation performance and potential in practical applications.

With the advent of dual carbon strategies, tremendous efforts have been made to create cellulose aerogel materials with excellent comprehensive performance [48,49]. Unfortunately, few cellulose aerogels have excellent flame-retardant, mechanical, and thermal insulation properties at the same time. In this study, TSP@Ca3 aerogels obtained by constructing a truss-like structure in a natural wood hollow tube exhibit excellent comprehensive performance. While enhancing the flame-retardant properties of cellulose-based aerogel materials, other key properties are not sacrificed. Meanwhile, we evaluate the raw material cost of TSP@Ca aerogel, and its preparation cost is about 130-200 \$ per cubic meter, which is lower than that of traditional cellulose aerogel. Besides, compared with the traditional petroleum-based insulation materials (RPUF or EPS) and reported cellulose-based aerogels (Table S3), TSP@Ca3 aerogel exhibits excellent bio-based, flame-retardant, mechanical, and thermal insulation properties (Fig. 7(h)). This is of vital significance for responding to the dual carbon strategy and advancing the application of cellulose-based thermal insulation materials in high-end emerging fields.

In addition, to intuitively study the fire safety performance of aerogel composites during actual fires, TODW and TSP@Ca house models were built to simulate the occurrence of fires. As shown in Fig. 7(i and j) and Videos S1 and S2, after the 1st ignition of TODW, the flame spreads rapidly, and the structure collapses. Notably, the TSP@Ca3 aerogel self-extinguishes after the 1st ignition. Even after four consecutive ignitions, it continued to selfextinguish while maintaining its structural integrity, demonstrating excellent fire safety performance. During the simulation process, the internal temperature of the house model was monitored in real time (Fig. 7(k)). When TODW is ignited for the first time, the temperature inside the model first rises and then falls. However, upon the second ignition, the internal temperature rises rapidly to 830.2 °C. In contrast, when the TSP@Ca3 aerogel is subjected to four ignitions, it still self-extinguishes, and the internal temperature shows no significant increase. These results confirm that TSP@Ca3 aerogel features excellent fire safety performance.

4. Conclusions

Inspired by the truss structure, this work successfully prepared a fire-safe, heat-insulating, high-strength, and fully biobased TSP@Ca aerogel by a dual cross-linking strategy. SA and PA were introduced into the TEMPO-oxidized wood template and replaced by Ca²⁺ to form a multi-point support structure, which was similar to "islands" or "nerve fibers". TSP@Ca aerogel exhibits higher compression performance (9.99 MPa) than TODW (3.92 MPa) due to its truss-like skeleton. Thanks to the introduction of PA and Ca²⁺, TSP@Ca aerogel features excellent fire safety, with a UL-94 V-0 grade and a high LOI of 43.3 %. Under strong heat radiation, TSP@Ca aerogel forms dense char layers to isolate the transfer of heat, oxygen, and combustible volatiles. Meanwhile, the Pand PO- radicals generated by the decomposition of TSP@Ca play an important role in the gas phase by trapping high-energy radicals. Therefore, the PHRR and THR of TSP@Ca aerogel are decreased from 946.8 kW/m² and 38.5 MJ/m² of TODW to 183.1 kW/m² and 13.2 MJ/m², respectively. The construction of an aerogel structure within TODW increases the heat conduction path, and thus the average thermal conductivity of TSP@Ca is reduced to 0.0561 W/(m K). In summary, this study provides a sustainable and rational strategy for the preparation of fully biobased wood aerogels with

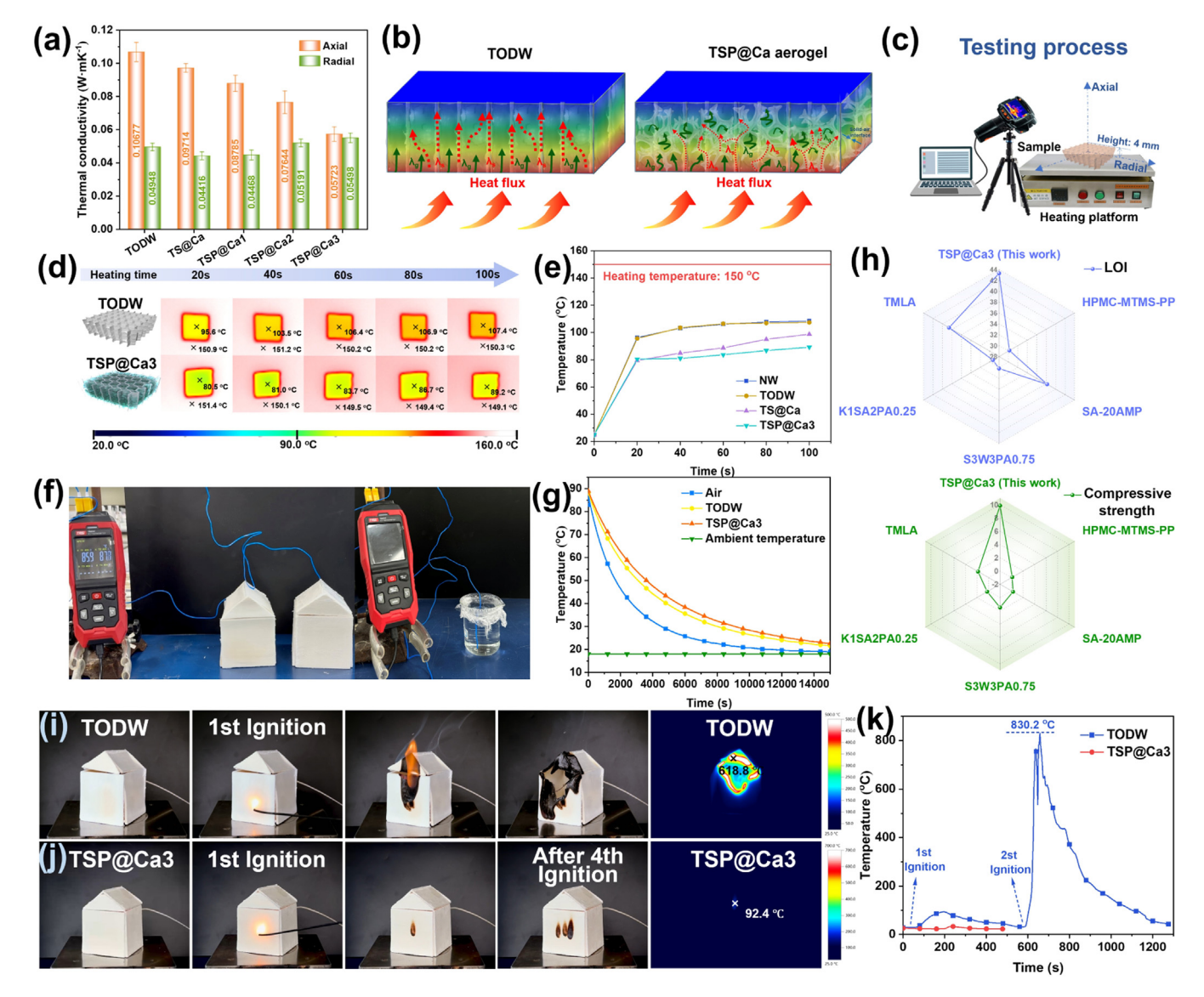


Fig. 7. (a) Thermal conductivity diagram of TODW, TS@Ca, and TSP@Ca aerogels. (b) Illustration of the thermal conductivity mechanism. (c) Simulation diagram of an infrared thermography test. (d) Top side pseudo-color thermal images of the TODW and TSP@Ca3 aerogels with a height of 0.4 cm after heating for 20, 40, 60, 80, and 100 s on a hot plate held at 150 °C. (e) Time-dependent temperature curves of the NW, TODW, TS@Ca, and TSP@Ca3 aerogels on the hot plate. (f) Thermal insulation performance simulation, and (g) temperature curves of the water in the air, TODW, and TSP@Ca3 during thermal insulation. (h) Comparison of the comprehensive performance of TSP@Ca3 aerogel prepared in this work with existing cellulose aerogels (Table S3). (i and j) Video Screenshot of the small house model simulating a fire, and the thermal imaging temperature distribution of the model. (k) Temperature curve during fire simulation.

excellent fire safety, thermal insulation, and ultra-high strength, which can find ubiquitous applications in various industries.

Declaration of competing interest

The authors declare that they have no known competing financial interests or personal relationships that could have appeared to influence the work reported in this paper.

CRediT authorship contribution statement

Yue Xu: Writing – original draft, Methodology, Investigation, Formal analysis, Data curation, Conceptualization. Shuhui Liang: Investigation, Conceptualization. Wanying Wang: Investigation. Chentao Yan: Methodology. Lubin Liu: Writing – review & editing, Project administration, Investigation, Formal analysis. Dawei Jiang: Supervision, Investigation. Min Hong: Supervision, Investigation. Miaojun Xu: Supervision, Resources, Investigation, Fund-

ing acquisition. **Bin Li:** Supervision, Funding acquisition. **Siqi Huo:** Writing – review & editing, Resources, Formal analysis.

Acknowledgements

This work was financially supported by the Natural Science Foundation of China (Nos. 52173069 and 52203082), the Northeast Forestry University "Double Ten Plan" Interdisciplinary Innovation Team for Young Teachers (2572025]T10), the Key Research and Development Projects in Heilongjiang Province (No. 2024ZXDXA29), Fundamental Research Funds for the Central Universities (No. 2572022BU02), Young Elite Scientist Sponsorship Program by Heilongjiang Province (No. 2023QNTJ006), Key Research and Development Projects in Heilongjiang Province (No. GZ20220056), Heilongjiang Postdoctoral Special Grant (No. LBH-TZ2402), Heilongjiang Postdoctoral Foundation (No. LBH-Z23047), and Undergraduate Innovation Project for Northeast Forestry University (No. 202410225365).

Supplementary materials

Supplementary material associated with this article can be found, in the online version, at doi:10.1016/j.imst.2025.09.044.

References

- J. Guo, S. Fu, Y. Deng, X. Xu, S. Laima, D. Liu, P. Zhang, J. Zhou, H. Zhao, H. Yu, S. Dang, J. Zhang, Y. Zhao, H. Li, X. Duan, Nature 606 (2022) 909–916.
- [2] C. Du, Y. Xu, C. Yan, W. Zhang, H. Hu, Y. Chen, M. Xu, C. Wang, B. Li, L. Liu, Sustain. Mater. Technol. 39 (2024) e00794.
- [3] B. Shi, Z.J. Xie, Y.J. Duan, G. Chen, Z.J. Li, H. Shen, Q. Chang, H.J. Wu, J. Mater. Sci. Technol. 236 (2025) 77–85.
- [4] J. Feng, Z. Ma, J. Wu, Z. Zhou, Z. Liu, B. Hou, W. Zheng, S. Huo, Y.-T. Pan, M. Hong, Q. Gao, Z. Sun, H. Wang, P. Song, Adv. Mater. 37 (2025) 2411856.
- [5] S. Cai, X. Deng, J. Beiyuan, X. Chen, D. Liu, D. Lv, C. Duan, L. Lin, R. Cha, W. Xie, H. Chen, J. Zhou, Z. Lu, L. Huang, W. Yuan, J. Build. Eng. 97 (2024) 110846.
 [6] T. Dey, L. Trasande, R. Altman, Z. Wang, A. Krieger, M. Bergmann, D. Allen,
- [6] T. Dey, L. Trasande, R. Altman, Z. Wang, A. Krieger, M. Bergmann, D. Allen, S. Allen, T.R. Walker, M. Wagner, K. Syberg, S.M. Brander, B.C. Almroth, Science 378 (2022) 841–842.
- [7] Z. Ma, J. Feng, S. Huo, Z. Sun, S. Bourbigot, H. Wang, J. Gao, L.-C. Tang, W. Zheng, P. Song, Adv. Mater. 36 (2024) 2410453.
- [8] Y. Wu, J. Chen, C. Xu, C. Chen, Chin. J. Chem. 43 (2025) 1691-1706.
- [9] Y. Shi, M. Wu, S. Ge, J. Li, A.S. Alshammari, J. Luo, M.A. Amin, H. Qiu, J. Jiang, Y.M. Asiri, R. Huang, H. Hou, Z.M. El-Bahy, Z. Guo, C. Jia, K. Xu, X. Chen, Nano-Micro Lett. 17 (2025) 3.
- [10] Z. Wang, X.F. Zhang, X. Kong, J. Yao, Chem. Eng. J. 490 (2024) 151518.
- [11] T. Zhang, J. Qu, J. Wu, F.-Z. Jiao, C. Li, F.-L. Gao, J. Liu, Z.-Z. Yu, X. Li, Adv. Funct. Mater. 34 (2024) 2403505.
- [12] M. Caniato, F. Bettarello, A. Ferluga, L. Marsich, C. Schmid, P. Fausti, Renew. Sust. Energ. Rev. 80 (2017) 585–596.
 [13] J. Song, C. Chen, Z. Yang, Y. Kuang, T. Li, Y. Li, H. Huang, I. Kierzewski, B. Liu,
- [13] J. Song, C. Chen, Z. Yang, Y. Kuang, T. Li, Y. Li, H. Huang, I. Kierzewski, B. Liu, S. He, T. Gao, S.U. Yuruker, A. Gong, B. Yang, L. Hu, ACS Nano 12 (2018) 140–147.
- [14] W. He, H. Qiang, S. Liang, F. Guo, R. Wang, J. Cao, Z. Guo, Q. Pang, B. Wei, J. Sun, Chem. Eng. J. 446 (2022) 137331.
- [15] T. Saito, S. Kimura, Y. Nishiyama, A. Isogai, Biomacromolecules 8 (2007) 2485–2491.
- [16] A. Isogai, T. Saito, H. Fukuzumi, Nanoscale 3 (2011) 71-85.
- [17] X. Zhou, L. Dong, S. Zheng, D. Cao, J. Chen, X. Feng, J. Zhu, X. Lu, L. Mu, Adv. Compos. Hybrid Mater. 8 (2025) 82.
- [18] X. Yu, H. Li, N. Kang, S. Lu, M. Xu, M. Wan, Adv. Sci. 12 (2025) e06808.
- [19] X. Yu, H. Li, X. Miao, N. Kang, W. Yao, M. Xu, Green Energy Environ. (2025), doi:10.1016/j.gee.2025.04.009.
- [20] X. Yu, H. Li, X. Miao, Ning Kang, Y. Sheng, Z. Xu, Z. Fu, M. Xu, R. Zong, S. Lu, Small 20 (2024) 2407060.

- [21] C. Wang, S.Q. Huo, G.F. Ye, Q. Zhang, C.F. Cao, M. Lynch, H. Wang, P.A. Song, Z.T. Liu, Chem. Eng. J. 500 (2024) 157418.
- [22] S. Ahankari, P. Paliwal, A. Subhedar, H. Kargarzadeh, ACS Nano 15 (2021) 3849–3874.
- [23] X. Wu, M. Liu, Xie. Lin, Cellulose 32 (2025) 1685-1698.
- [24] Y. Wang, Y. Zhang, J. Du, Y. Tao, J. Hu, Y. Lv, J. Lu, C. Fu, H. Wang, Z. Yuan, Adv. Compos. Hybrid Mater. 8 (2025) 11.
- [25] Y.J. Xu, K.T. Zhang, J.R. Wang, Y.Z. Wang, Adv. Mater. 37 (2025) 2414880.
- [26] X. Yu, H. Li, K. Qiu, S. Lu, SmartMat 5 (2024) e1275.
- [27] H.L. He, Q. Jiang, Y.H. Wan, M.H. Mia, X.R. Qu, M. Zhou, X.Y. He, X.Q. Li, M. Hong, Z.C. Yu, S.Q. Huo, J. Mater. Sci. Technol. 205 (2025) 257–271.
- [28] D. Ye, C. Chang, L. Zhang, Biomacromolecules 20 (2019) 1989–1995.
- [29] J. Zhu, Y. Wang, X. Zhao, N. Li, X. Guo, L. Zhao, Y. Yin, Int. J. Biol. Macromol. 267 (2024) 131450.
- [30] S.W. Cranford, A. Tarakanova, N.M. Pugno, M.J. Buehler, Nature 482 (2012) 72–91.
- [31] J.H. Kiang, Avian Wing Bones, Ph.D. Thesis, University of California, 2013.
- [32] S. Lin, L. Chen, M. Zhang, Y.M. Xie, X.D. Huang, S.W. Zhou, Adv. Eng. Softw. 149 (2020) 102905.
- [33] Z. Sun, T. Cui, Y. Zhu, W. Zhang, S. Shi, S. Tang, Z. Du, C. Liu, R. Cui, H. Chen, X. Guo, Sci. Rep. 8 (2018) 13859.
- [34] D. Xing, W. Chen, L. Zhao, J. Ma, Sci. China-Technol. Sci. 55 (2012) 2091–2098.
- [35] K. Srinivasan, K. Selvakumar, Indian J. Eng. Mater. Sci. 29 (2022) 428–431.
- [36] Y. Guo, Q. Yang, S. Huo, J. Li, P. Jafari, Z. Fang, P. Song, H. Wang, Prog. Polym. Sci. 162 (2025) 101935.
- [37] G. Ye, S. Huo, C. Wang, Q. Zhang, H. Wang, P. Song, Z. Liu, Small 20 (2024) 2404634.
- [38] C. Bai, X. Yang, D. Liu, J. Wu, Y. Wang, Y. Lu, T. Wu, P. Jiang, X. Wang, Chem. Eng. J. 500 (2024) 156740.
- [39] H. Yan, J. Wang, C. Du, Z. Li, H. Yuan, Z. Xu, Y. Tan, Adv. Mater. 36 (2024) 2400648.
- [40] M. Rinaudo, Macromol. Biosci. 6 (2006) 590-610.
- [41] Y. Gang, Y. Xu, A. Qin, Q. Li, C. Yan, W. Zhang, M. Xu, K. Xu, B. Li, L. Liu, Chem. Eng. J. 500 (2024) 157446.
- [42] T. Sai, X. Ye, B. Wang, Z. Guo, J. Li, Z. Fang, S. Huo, J. Mater. Sci. Technol. 225 (2025) 11–20.
- [43] Y. Xu, H. Hu, B. Tao, R. Yin, L. Liu, B. Li, Constr. Build. Mater. 484 (2025) 141876.
- [44] Y. Shi, Y. Xu, K. Xu, C. Yan, B. Li, L. Liu, Chem. Eng. J. 498 (2024) 155181.
- [45] Y. Si, J. Yu, X. Tang, J. Ge, B. Ding, Nat. Commun. 5 (2014) 5802.
- [46] F. Hu, S. Wu, Y. Sun, Adv. Mater. 31 (2019) 1801001.
- [47] Y. Xu, C. Yan, C. Du, K. Xu, Y. Li, M. Xu, S. Bourbigot, G. Fontaine, B. Li, L. Liu, Compos. Pt. B-Eng. 261 (2023) 110809.
- [48] W. Chen, H. Yu, S.-Y. Lee, T. Wei, J. Li, Z. Fan, Chem. Soc. Rev. 47 (2018) 2837–2872.
- [49] R.T. Olsson, M.A.S.A. Samir, G. Salazar-Alvarez, L. Belova, V. Strom, L.A. Berglund, O. Ikkala, J. Nogues, U.W. Gedde, Nat. Nanotechnol. 5 (2010) 584–588